Self-Excited Diode Rectifying Wound-Field Synchronous Motor Utilizing Space Harmonics and Flux-Intensifying with Carrier Harmonics

Masahiro Aoyama / IEEE Member
Shizuoka University
3-5-1 Johoku, Naka-ku, Hamamatsu, Shizuoka JAPAN
aoyama.masahiro@shizuoka.ac.jp

Toshihiko Noguchi / IEEE Senior Member
Shizuoka University
3-5-1 Johoku, Nakaku, Hamamatsu, Shizuoka JAPAN
noguchi.toshihiko@shizuoka.ac.jp

***Abstract*—This paper describes a novel self-excitation technique in which space harmonics and carrier harmonic is effectively utilized for the field magnetization instead of permanent magnets. The unique point of this technique are the following points. The second-order space harmonic that is structurally unavoidably generated in the motor with concentrated winding stator is utilized for self-excitation by inductive coupling. Secondary, the carrier harmonics inevitably generated in motor controlled by inverter are utilized for flux-intensifying by inductive resonance coupling. After explaining the proposed new self-excitation principle, then, the prediction of driving characteristics by electromagnetic field analysis (FEA) is shown. In particular, the effect of value of the carrier frequency to be magnetically resonant coupled and the torque improvement effect by the flux-intensified electromagnet are clarified. Consequently, it has been clarified that the proposed new permanent- magnet free motor can improve the torque density in the low-speed area because the carrier harmonic can generates the large electromangetomotive force in rotor winding by inductive resonance coupling.**

Keywords— wound-field, self-excitation, space harmonics, carrier harmonics, inductive resonance coupling .

I. Introduction

An electric vehicle development is actively carried out today as environmental pollution reduction technology in the transportation equipment field [1]-[3]. As the key technologies for developing electric vehicles, there are a motor for traction, an inverter for efficiently converting electric power, and a battery for energy storage. The motor that is one of the key technologies mainly adopts a permanent magnet type synchronous motor and an induction motor, and the optimum motor is selected according to the driving performance required for its electric car and its systems. In particular, the permanent magnet type synchronous motors (PMSM) are adopted as many electric vehicle traction motors because of their features of high torque density, wide high efficiency area, and small size and light weight [4],[5]. Generally, permanent magnet (PM) machines can generate the high torque density with a high permanent magnet flux density in the rotor. Thus, the greater the magnetic flux density the lower armature current required to generate a given torque. However, a consequence of increasing flux density of such machines have a higher back EMF constant which is a linear product of the flux density and the rotation speed. To solve the drawback of that problem, a variable magnetic flux synchronous motors that can control the magnetic flux of the PMs are intensively investigated both in industries and in academia a next generation PMSM [6]-[12]. Furthermore, ultimately, it is desirable to achieve the same performance as the PM type motor with the PM-free motor that does not use expensive PMs. As a classical technique, an induction motor (IM) can be cited as the motor realizing a full-rage variable magnetic field with the PM-free motor [13],[14]. However, in the case of the IM, it is necessary to continuously supply the exciting magnetic flux from the primary side and there is a problem that the torque and the power factor are low compared with PMSM. As a technique capable of realizing torque improvement and power factor improvement over a classical IM, the induced electromotive force supplied from the primary side is rectified in the rotor to form the DC magnetic flux, and an electromagnet is constructed to be driven as a synchronous motor. Such self-excited wound-field type motor are designed to deliberately excite time harmonic on three-phase armature current to self-excite them, or by devising winding pitch of distributed winding stators to intentionally generate space harmonic[15]-[19]. On the other hand, the authors focused on the fact that the second-order space harmonic inevitably occurs due to the concentrated winding stator structure, and proposed the unique self-excited wound-field motor utilizing space harmonic in the past [20],[21]. Furthermore, it carries out verification of actual machine, already verifying its principle and its usefulness [20],[21]. However, this motor can not obtain the sufficient induced electromotive force at extremely low rotation speed area, and the problem of low torque at this operation area is clear from the actual machine verification. In the view of these problems, this paper proposes a new motor that achieves torque improvement in the low rotation speed range of this motor by flux-intensifying with carrier harmonics.

II. Operation Principle of Proposed Motor

Figure 1 shows a cross section diagram of the proposed motor designed with a small capavity in anticipation of actual

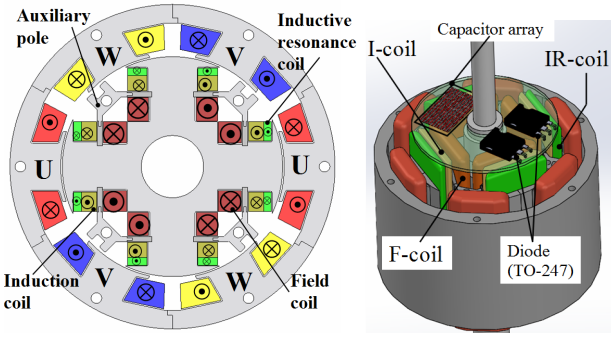

(a) Cross section diagram. (b) Prototype structure.

Fig. 1. Proposed motor.

Table I. Specifications of prototype.

Stator outer diameter (mm)	125
Stack length (mm)	80
Pole pairs	2
Number of stator slots	6
Armature winding resistance (Ω/coil)	2.0
Induction-coil resistance (Ω/coil)	1.4
Field-coil resistance (Ω/coil)	1.4
Inductive-resonance coil resistance (Ω/coil)	0.4
Number of Induction-coil turn	110
Number of Field-coil turn	110
Number of Inductive-resonance-coil turn	20

machine verification in our university's lab. This proposed motor has a stator core outer diameter of ϕ125, a stack length of 80 mm, and a stator winding resistance of 2.0 Ω/pole as shown in Table I. The salient pole rotor is enclosed in the concentrated winding stator, and the salient pole motor has three type of rotor coils, that is, the induction coil (I-coil) for obtaining the induced electromotive force from the space harmonic, the field coil (F-coil) for generating the field flux via the diode rectifier circuit and the inductive resonance coil (IR-coil) with the carrier harmonics. Figure 2 (a) shows the distribution of the second-order space harmonic calculated by electromagnetic field analysis. The electromagnetic field analysis used commercial software (JMAG-Designer). As shown in this figure, it is found that second-order space harmonic unavoidably generated in the concentrated winding stator structure interlink a lot in the vicinity of the gap of the rotor salient pole, and by arranging the I-coil on the gap side, it is effective to obtain the induced electromotive force. In addition, an auxiliary poles are arranged between the salient poles (on q-axis) so that the space harmonic frequently interlinks with the rotor salient poles. Figure 2 (b) shows the carrier harmonic distribution of the proposed motor when the inverter is driven at the carrier frequency of 2 kHz. As can be seen from this figure, it is confirmed that the rotor salient poles interlink a lot carrier harmonic as same as the second-order space harmonic. In addition, as shown in this figure, since the flux linkage is distributed near the gap in the carrier harmonic, IR-coil is placed on the outer diameter side of the rotor as shown in Fig. 1, aiming to increase the amount of flux linkage of carrier harmonics. On the other hand, the amplitude of the

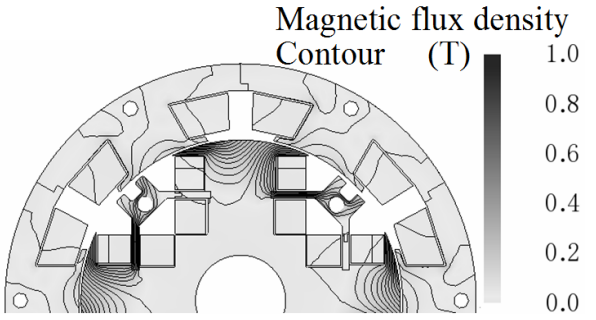

(a) Second-order space harmonic.

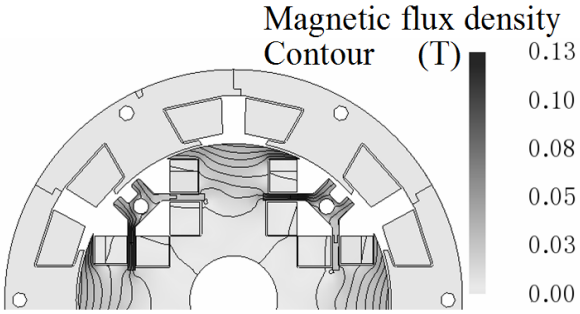

(b) Carrier harmonic (2 kHz).

Fig. 2. Harmonic flux distribution.

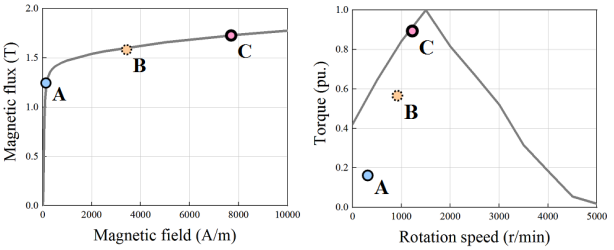

(a) B-H curve of iron core. (b) Operation point.

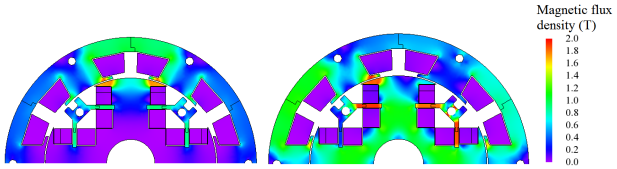

(c) Point : A. (d) Point : B.

Fig. 3. Driving point and magnetic flux density with respect to its point.

carrier harmonic is smaller than that of the space harmonic. However, since the time change rate of the magnetic flux is large, if the magnetic coupling with respect to the carrier harmonic can be improved, the torque can be improved in the low rotation speed area. In the view point of this, the attention has focused on wireless power transmission technique based on the magnetic field resonance coupling that has been extensively studied for commercialization in recent years [22]. This is, self-excitation by the carrier harmonics can be realized by configuring an LC series resonance circuit whose resonance frequency is set on the carrier frequency. The carrier harmonic

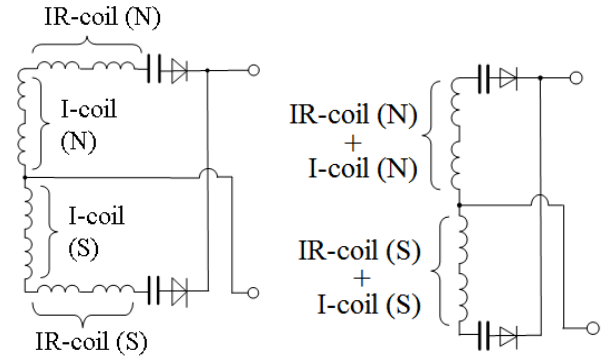

(a) Series connection type. (b) Integrated coil type.

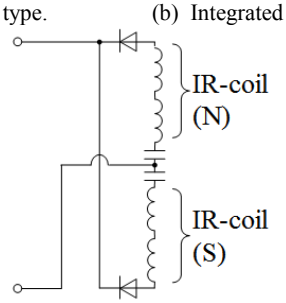

(c) Parallel connection type.

Fig. 4. Connection type of I-coil and IR-coil.

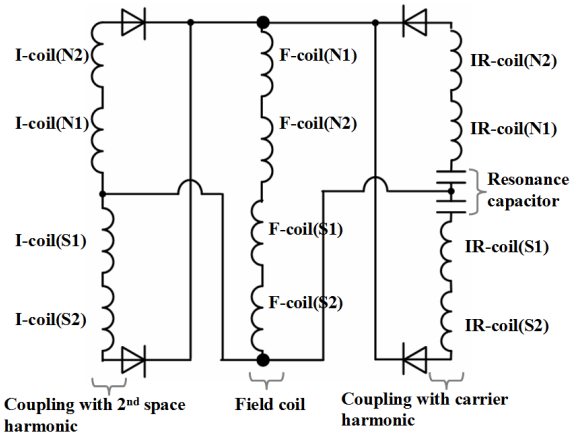

Fig. 5. Rotor winding circuit.

is inevitably generated in the motor control driven by PWM control inverter.

Then, the configuration of the rectifier circuit of the rotor winding will be described. As described above, although the carrier harmonic is resonantly coupled by magnetic field, on the other hand, it becomes high impedance at non-resonance, organizing self-excitation become difficult. Since, the proposed motor classified variable field motor, the *d*-axis inductance varies dynamically as shown in Fig. 3. This means that the resonance frequency fluctuates with respect to inductance fluctuation. In the purpose of improving the torque in the low rotation speed range, when the value of the resonance capacitor is selected with the carrier harmonic frequency by using the inductance value at the low rotation speed range, it is assumed that the resonance state becomes non-resonant state with

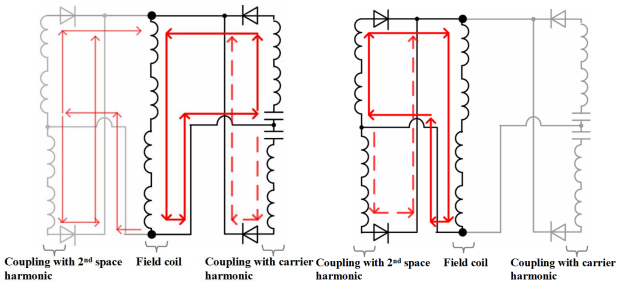

(a) Under low-rotation speed. (b) Over middle-rotation speed.

Fig. 4. Rotor winding circuit passively switched at rotation speed.

respect to the rotation speed increases. Here, there are three possible connection type for I-coil and IR-coil rotor windings, as shown in Fig. 4. Since the Fig. 4 (a) and (b) are wound on the same salient pole, the performance does not change equivalently. Figure 4 (c) is different from the series connection of I-coil and IR-coil, and IR-coil and I-coil are connected in parallel. Figure 5 shows the rotor winding circuit in which the IR-coil of Fig. 4 (c) is connected in parallel with the I-coil to the F-coil through diode rectification respectively. Here, in order to avoid high impedance at non-resonance and inability to self-excite, it is desirable that the I-coil for self-excitation with the second-order space harmonic ant the rotor resonantly coupled with the carrier harmonic, that is inductive resonance coil (IR-coil), are connected in parallel to the field coil (F-coil) via diodes, respectively. Therefore, the system of Fig. 4 (c) is adopted, and the rotor circuit configuration shown in Fig. 5 is used. Here, since the F-coil is the coil forming the field pole, it is not desirable that the harmonic flux interlinks to generate an induced electromotive force. Therefore, by arranging the coils on the inner diameter side of the rotor, it is possible to prevent the linkage of harmonic magnetic fluxes and to form the field of the constant magnetomotive force. With such the circuit configuration, as shown in Fig. 6, the field pole is self-excited with carrier harmonic in the low rotation region to form the field pole under resonant state with carrier harmonic, and self-excited with the space harmonic at the medium rotation or more to self-excite the field pole under non-resonant state. That is, the circuit self-excited by carrier harmonics and the circuit self-excited by space harmonic are switched passively.

III. Operation Characteristics

A. Flux-Intensifying with Carrier Harmonic

As explained in the previous chapter, the I-coil obtains an induced electromotive force by electromagnetic inductive coupling, while the IR-coil utilize the carrier harmonics as the resonance frequency to form an LC series resonant circuit, and obtains an induced electromotive force by inductive resonance coupling. That is, in the proposed motor, magnetic resonance coupling is performed in the LC series resonance circuit in which the carrier frequency F_c is used as the resonance frequency F_{res}. In the past, the carrier harmonics inevitably generated by an inverter-driven motor become a source of iron loss and conductor eddy current loss in the armature winding,

and the motor performance is degraded. However, this proposed technique can be utilized to improve torque. As shown in Eq. (1), F_r is determined by the combination of the self-inductance of IR-coil L_{IR} and the resonant capacitance C, but as shown in Fig. 1 (b), it is preferable to fix the capacitor array on the rotor without changing the capacitance.

$$F_r = F_c = \frac{1}{2\pi\sqrt{LC}} \tag{1}$$

Since the impedance Z_{IR} of the LC series resonant circuit is represented by Eq. (2) during non-resonance, the impedance is high. Here, R_{IR} is the winding resistance value of L_{IR}.

$$Z_{IR} = R_{IR} + j\left(\omega L_{IR} - \frac{1}{\omega C}\right) \tag{2}$$

As a preliminary study, the carrier frequency is set to 2 kHz, the torque characteristics in the low-rotation speed range are compared between the case where the LC series resonance circuit of Fig. 3 (b) is impedance-matched with the resonance frequency at 2 kHz and the case of the non-resonance case. Figure 6 shows the torque characteristics when the armature magnetomotive force is 389 AT (armature current 5 A_{pk}) and only the electromagnet torque (d-axis current i_d = 0 control), and Fig. 6 shows the comparison result of the torque ripple. Here, the rotor salient pole is defined by d-axis, the interval between the salient pole is defined by q-axis. The non-resonance state (circuit without resonance capacitance in Fig. 5) is the same as the model in the conventional case of self-excitation with space harmonics, so it is described as "conventional" in each figure. From both figures, in addition to the improvement of average torque (for example, +36.6 % at 100 r/min, +28.7 % at 200 r/min, +11.9 % at 400 r/min, and +7.7 % at 1000 r/min), it is possible to confirm the reduction of torque ripple. Here, in Fig. 7, the conventional model as T_{rc}, and the proposed model as T_{rp}. The torque ripple is defined by dividing the difference between the instantaneous maximum torque and the instantaneous minimum torque by the average torque in the range of one electrical angle cycle. From this figure, it is T_{rp} = 76.0 % with respect to T_c = 95.7 % at 400 r/min. As described above, in the motor, the d-axis inductance largely fluctuates with the rotation speed according to the variable field principle. As can be seen from Fig. 6, since impedance matching was performed with the inductance of 100 r/min to improve torque in the low rotation range, it deviated from the resonance point as the rotation speed increased, and the flux intensifying effect due to carrier harmonics was reduced. With regard to torque ripple, it is possible to reduce torque ripple by being able to reduce the permeance fluctuation by increasing the amount of rotor magnetization due to the flux-intensifying effect by carrier harmonics. The above can be confirmed from Fig. 8 because the field current of the proposed model is increased compared to the conventional model. In order to analyze the above in more detail, Fig. 9 shows the results of evaluating the torque waveform by Fourier series expansion and evaluating each harmonic component, and Fig. 10 shows the results of harmonic analysis of the field current. From these two figures, although the difference is not seen in the harmonic component of the field current, on the other hand, in the 6th and 12th

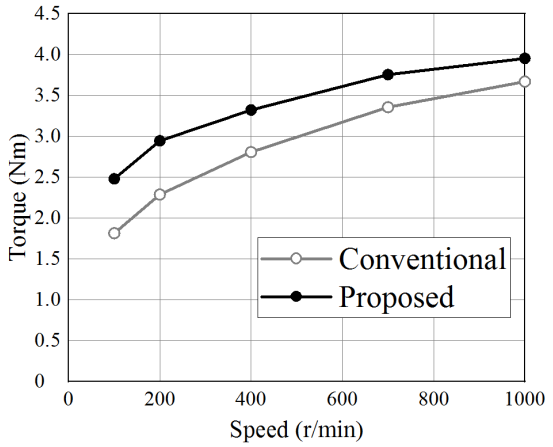

Fig. 6. Torque characteristics with respect to rotation speed under 389 AT under i_d = 0 control .

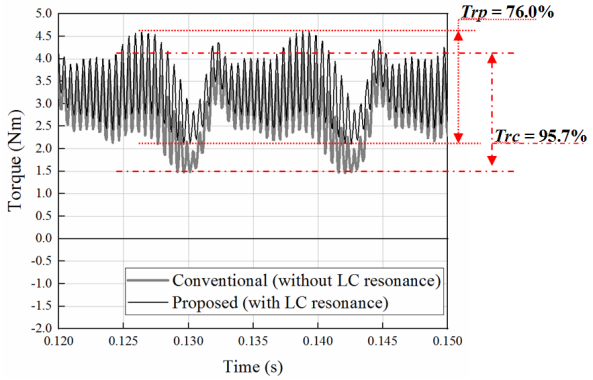

Fig. 7. Torque ripple under 389 AT (i_d = 0) at 400 r/min.

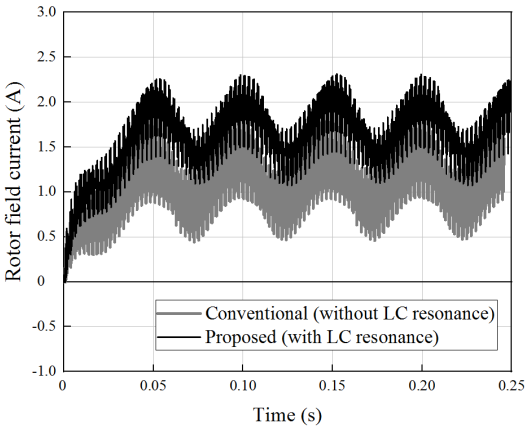

Fig. 8. Rotor field current under 389 AT (i_d = 0) at 400 r/min.

harmonic of the electrical angle, the proposed model is smaller than the conventional model. When comparing the gap flux density waveform from Fig. 11, the gap flux density is higher in the proposed model. Especially, in the section of 45 deg to 75 deg of rotor position at the momentary maximum torque and in the section of 100 deg to 130deg of rotor position at the momentary minimum torque, circumferential electromagnetic

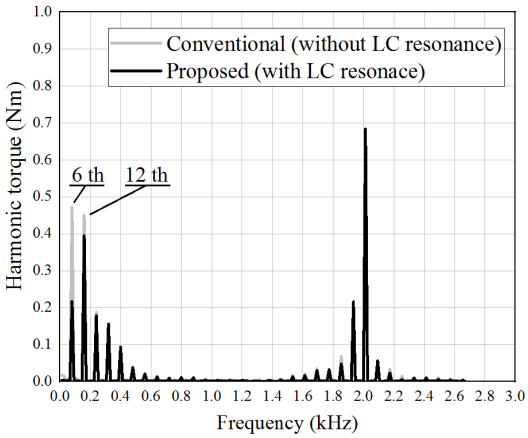

Fig. 9. Harmonic contents of torque under 389 AT at 400 r/min.

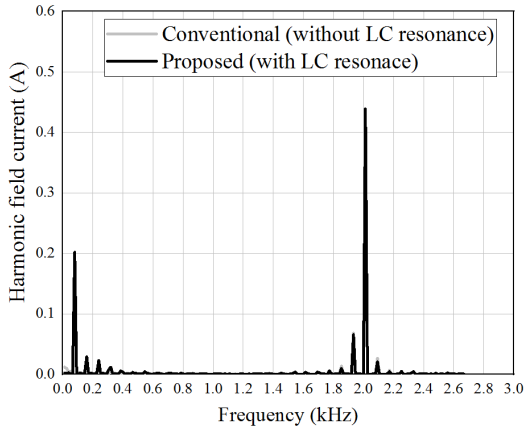

Fig. 10. Harmonic contents of field current under 389 AT at 400 r/min.

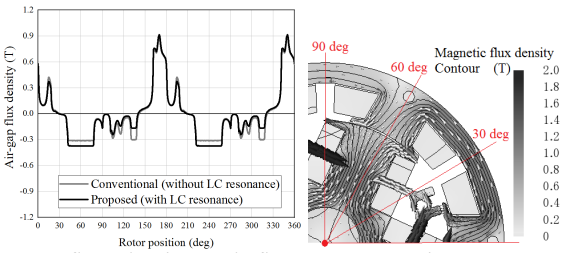

(a) Gap-flux density and flux vectors at instantaneous maximum torque.

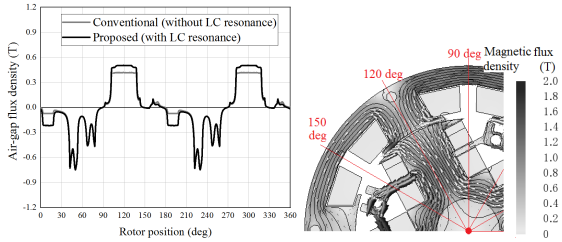

(a) Gap-flux density and flux vectors at instantaneous minimum torque.

Fig. 11. Air-gap flux density with respect to rotor position.

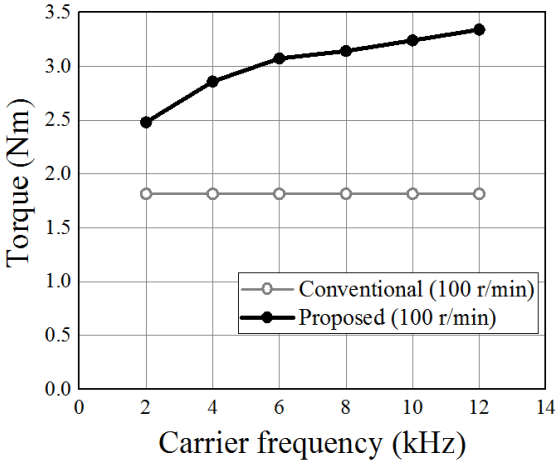

Fig. 12. Torque characteristics with respect to resonant frequency under 389 AT at 100 r/min.

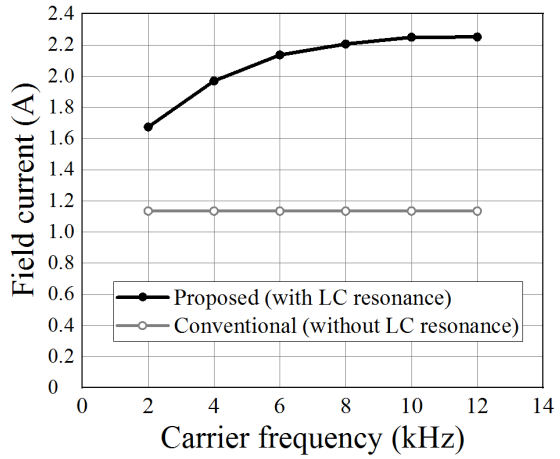

Fig. 13. Field current characteristics with respect to resonant frequency under 389 AT at 100 r/min.

force is hardly generated and radial electromagnetic force is dominant. Since the gap magnetic flux density of the proposed model is high at the above rotor position, the amount of magnetization of the field pole is increased by the flux-intensifying effect by the carrier harmonics, and the permeance fluctuation due to the double salient pole structure is reduced. As a result, it is considered that the torque ripple can be reduced.

B. Relationship between Carrier Frequency and Drive Characteristics

Next, the carrier frequency F_c is changed. At the same time, the resonant capacitance C is changed to maintain $F_r = F_c$. The relationship with the torque characteristic at the time is predicted by electromagnetic field analysis. In the previous section, the drive characteristics at carrier frequency $F_c = 2$ kHz are shown, but in this section, torque characteristics are shown in Fig. 12 when the carrier frequency F_c is changed with the rotation speed $N = 100$ r/min fixed, that is, when the

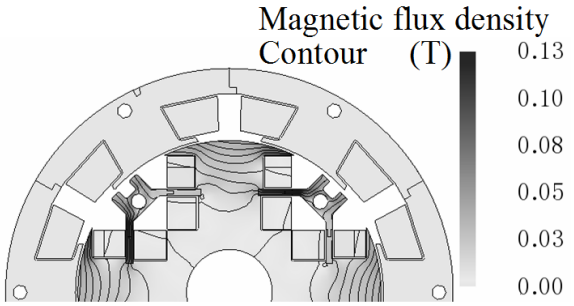

(a) Carrier frequency F_c = 2 kHz.

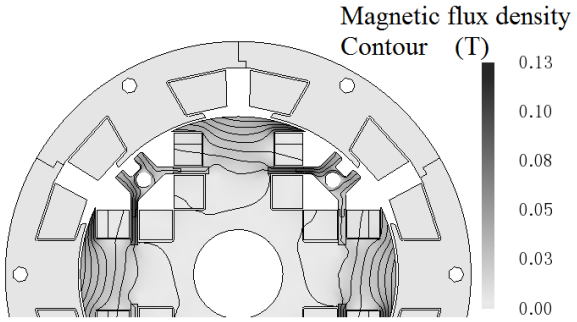

(b) Carrier frequency F_c = 4 kHz.

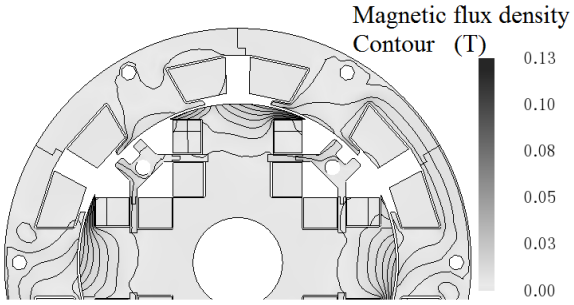

(c) Carrier frequency F_c = 12 kHz.

Fig. 14. Harmonic flux distribution with respect to carrier frequency.

resonance frequency F_r is changed. From this figure, the average torque is +57.5 % at F_c = 4 kHz, +69.2 % at F_c = 6 kHz, +73.0 % at F_c = 8 kHz, +78.5 % at F_c = 10 kHz and +84.0 % at F_c = 12 kHz, respectively. Figure 13 shows the average value of the field current corresponding to Fig. 12. From this figure, the average value of the field current increases with the increase of the carrier frequency, and from this result, the induced EMF in the IR-coil which is magnetically coupled at the carrier frequency increases by increasing the carrier frequency F_c. As a result, it can be seen that the torque increases because the field current increases and the amount of magnetization of the field pole increases. On the other hand, it is expected that the average value of the torque and the field current will increase in a linear relationship because the time change of the magnetic flux increases in proportional to the carrier frequency F_c, but as can be seen from Fig. 12 and Fig. 13, it is actually confirmed that have non-linearity. As this factor, as shown in Fig. 14, the

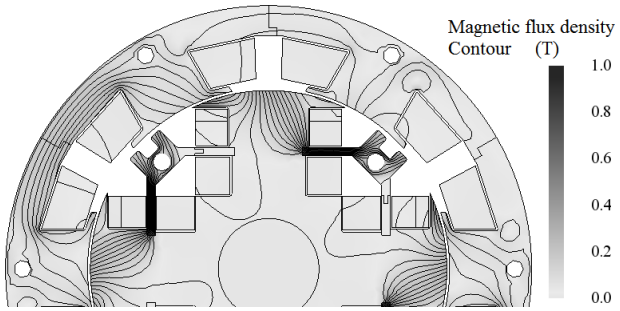

Fig. 15. Second space harmonic distribution at carrier frequency 12 kHz.

carrier harmonics flux linked to the rotor salient pole decreases in proportional to the carrier frequency, and as a result, it can be considered that the amount of carrier harmonic linkage flux linked to the IR-coil decreases and the induced electromotive force does not increases linearly. This result means that when the proposed motor is intensified field magnetization utilizing carrier harmonics, the optimum carrier frequency exists with the system efficiency including the torque and the inverter. These examinations will be verified in the actual machine evaluation test using a prototype in the near future.

C. Amplitude Modulation of Induced Electromotive Force

In addition to the determination of the resonance frequency F_r in the previous section, the Q factor is mentioned as an important design item that influences the flux-intensifying effect by the carrier harmonics of the proposed motor. In this motor, the second space harmonic and the carrier harmonics are respectively linked to the rotor salient pole, and in the I-coil or IR-coil, the electromotive force is obtained from the respective harmonic fluxes. As shown in Fig. 15, there is no difference in the distribution of space harmonics even when the carrier frequency F_c is changed. Therefore, in the IR-coil, depending on the Q value, the amplitude modulation occurs in which the amplitude of the carrier harmonic changes gradually in time due to the second space harmonic (it is third time harmonic on the dq-axis reference frame on the rotor). It means that the second space harmonic correspond to the envelope of the modulated waveform. Assuming that the carrier harmonic and the third time harmonic (it means that observation of the second space harmonic from the fundamental wave synchronous rotation coordinate) are ψ_c and ψ_{3rd}, respectively, it can be written as the following equation. Therefore, the sideband waveform ψ_{IR} of the magnetic flux linked to IR-coil is as shown in Eq. (5).

$$\psi_c = \phi_c \cos \omega_c t \tag{3}$$

$$\psi_{3rd} = \phi_{3rd} \cos \omega_{3rd} t \tag{4}$$

$$\begin{aligned} \psi_{IR} &= \psi_c \cdot \psi_{3rd} \\ &= \frac{\phi_c \phi_{3rd}}{2} \{\cos(\omega_c + \omega_{3rd})t + \cos(\omega_c - \omega_{3rd})t\} \end{aligned} \tag{5}$$

In Eq. (5), as an example, when ψ_c = 12566.4 rad/s (F_c = 2 kHz) and ψ_{3rd} = 83.8 rad/s (rotor rotation speed 400 r/min,

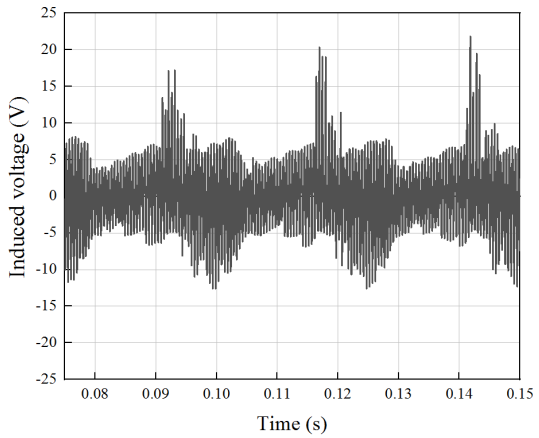

(a) Induced voltage in IR-coil with open windings.

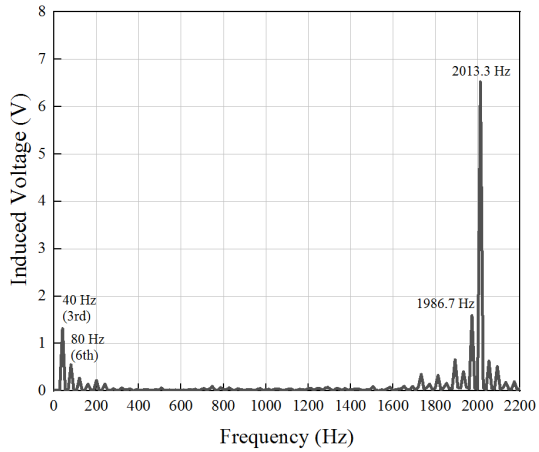

(b) Harmonic contents.

Fig. 15. Induced voltage in IR-coil with open-windings at carrier frequency 2 kHz under 389 AT and 400 r/min.

13.3 Hz), the sideband of ψ_{IR} is becomes 1986.7 Hz and 2013.3 Hz. In Fig. 10 and Fig. 16, it can be confirmed that the above-mentioned sideband components are generated in addition to the carrier frequency F_c = 2 kHz. From the above, it is understood that the Q factor is an important design parameter that affects the performance in the motor. Next, under the conditions of rotor rotation speed 100 r/min, armature magnetomotive force 389 AT, and the carrier frequency F_c = 2 kHz, the capacitance of the resonant capacitance is changed. In other words, the resonant frequency and the carrier frequency do not match ($F_c \neq F_{res}$). And the effect on the torque was obtained, and the torque characteristics were determined by electromagnetic field analysis. The result is shown in Fig. 16. From this figure, it can be seen that in the current design, there is no significant change in the torque characteristics even if it deviates from the resonance frequency in the range of about ±300 %. On the other hand, it can also be inferred that the torque characteristics change by designing the Q factor further from the current design.

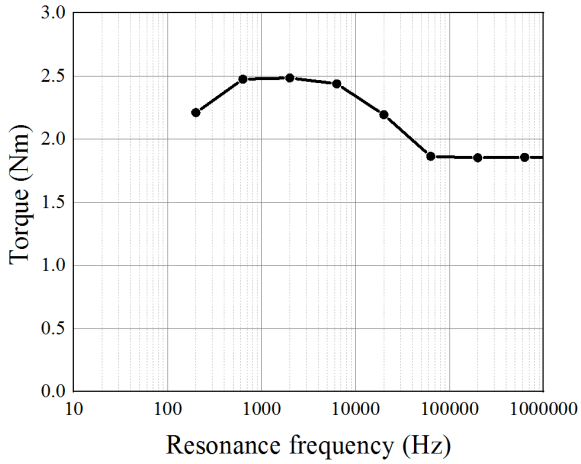

Fig. 16. Resonance frequency-vs.-torque characteristics at carrier frequency 2 kHz under 389 AT and 100 r/min.

IV. Conclusion

The purpose of this research is to improve the torque in the low speed range of the wound-field type synchronous motor self-excited by the second-order space harmonics that is inevitably generated in the concentrated winding stator structure. In this paper, the motor has been proposed that utilizes the inductive magnetic resonance coupling principle to obtain an electromotive force from the carrier harmonics that is inevitably generated when driving an inverter to intensify the field. The technique of the rotor winding circuit which can be used together with obtaining electromotive force from carrier harmonics by inductive magnetic resonance coupling was explained, acquiring elecromotive force from the second-order space harmonic by electromagnetic induction coupling. Then, the proposed principle was verified by FE-analysis. In addition, the torque characteristics were predicted when the carrier frequency was changed, and the relationship between the carrier frequency and the torque characteristics was clarified. The future plain is to verify the proposed technique using the prototype for proof of principle. Furthermore, the drive characteristics (torque, adjustable speed, efficiency map, etc.) are clarified experimentally. Then, examination of the optimum carrier frequency including the system efficiency and the control method for changing the carrier frequency to the optimum according to the resonance state are considered.

References

[1] U. Keller, T. Godecke, M. Weiss, C. Enderle and G. Henning, “Diesel Hybrid -The Next Generation of Hybrid Powertrains by Mercedes-Benz-,” 33rd International Vienna Motor Symposium 2012.

[2] Y. Sato, S. Ishikawa, T. Okubo, M. Abe and K. Tamai, “Development of High Response Motor and Inverter System for the Nissan LEAF Electric Vehicle,” *SAE Technicall Paper*, No. 2011-01-0350, 2011.

[3] F. Momen, K. Rahman, Y. Son and P. Savagian, “Electrical Propulsion System Design of Chevrolet Bolt Battery Electric Vehicle,” *IEEE Energy Conversion Congress and Expo (ECCE)*, 2016.

[4] S. Jurkovic, K. M. Rahman, P. Savagian, and R. Dawsey, “Electric Traction Motors for Cadillac CT6 Plugin Hybrid-Electric Vehicle,” *SAE International Technical Paper*, No. 2016-01-1220.

[5] S. Jurkovic, K. Rahman, B. Bae, N. Patel, and P. Savagian, "Next Generation Chevy Volt Electric Machines; Design, Optimization and Control for Performance and Rare-Earth Mitigation," in *IEEE 2016 Energy Conversion Congress and Exposition* (*ECCE*), 2016, pp. 5219-5226.

[6] V. Ostovic, "Memory Motors - a New Class of Controllable Flux PM Machines for a True Wide Speed Operation," *Proc. of IEEE Industry Applications Society Conference*, vol. 4, pp. 25772584, 2001.

[7] T. Kato, N. Limsuwan, C. Y. Yu, K. Akatsu and R. D. Lorenz, "Rare Earch Reduction Using a Novel Variable Magnetomotive Force, Flux Intensified IPM Machine," *IEEE Trans. on IA*, vol. 5, no. 3, pp. 1748-1756, May/June, 2016.

[8] T. Mizuno, K. Nagayama, T. Ashikaga and T. Kobayashi, "Basic Principles and Characteristics of Hybrid Excitation Synchronous Machine," *Electrical Engineering in Japan*, vol. 117, no. 5, pp. 110-123, 1996.

[9] J. A. Tapia, F. Leonardi and T. A. Lipo, "Consequent-Pole Permanent-Magnet Machine with Extended Field-Weakening Capability," *IEEE Trans. on IA.,* vol. 39, no. 6, pp. 1704-1709, 2003.

[10] M. Namba, K. Hiramoto and H. Nakai, "Novel Variable-Field Machine with a Three-Dimensional Magnetic Circuit," *IEEE Trans. on IA.,* vol. 53, no. 4, pp. 3403-3410, 2017.

[11] A. Athavale, T. Fukushige, T. Kato, C. Y. Yu and R. D. Lorenz, "Variable Leakage Flux (VLF) IPMSMs for Reduced Losses over a Driving Cycle while Maintaining the Feasibility of High Frequency Injection-Based Rotor Position Self-Sensing," *IEEE Energy Conversion Congress and Exposition (ECCE),* 2014.

[12] I. Urquhart, D. Tanaka, R. Owen, Z. Q. Zhu, J. B. Wang and D. A. Stone, "Mechanically Actuated Variable Flux IPMSM for EV and HEV Applications," *Proc. of EVS27 International Battery, Hybrid and Fuel Cell Vehicle Symposium 2013,* pp. 0684-0695, 2013.

[13] O. Mores, J. Richnow and D. Gerling, "New Cost Effective Concentrated Winding Topology for Induction Machines," ANSYS Conference & 32nd CADFEM User's Meeting, 2014.

[14] M. Kondo, R. Ebizuka and A. Yasunaga, "Rotor Design for High Efficiency Induction Motors for Railway Vehicle Traction," 2009 International Conference on Electrical Mechanical Machines and Systems (ICEMS2009), 2009.

[15] J. Oyama, S. Toba, T. Higuchi and E. Yamada, "The Principle and Fundamental Characteristics of Half-Wave Rectified Brushless Synchronous Motor," *IEEJ Trans. on IA.*, vol. 107, no. 10, pp. 1257-1264, 1987. (in Japanese)

[16] J. Oyama, T. Higuchi, N. Abe and E. Yamada, "The Principle and Fundamental Characteristics of AC-Excited Brushless Synchronous Motor," *IEEJ Trans. on IA.*, vol. 109, no. 7, pp. 515-522, 1989. (in Japanese)

[17] T. Fukami, K. Taka, T. Miyamoto and F. Shibata, "A New Self-Excitation Scheme for Three-Phase Synchronous Generators," *IEEJ Trans. on IA.*, vol. 114, no. 11, pp. 1083-1089, 1994. (in Japanese)

[18] T. Fukami, Y. Hanada and T. Miyamoto, "Analysis of the Self-Excited Three-Phase Synchronous Generator Utilizing the 2nd-Space Harmonic for Excitation," *IEEJ Trans. on IA.*, vol. 117, no. 1, pp. 57-65, 1997. (in Japanese)

[19] C. Stancu, T. Ward, K. Rahman, R. Dawsey, and P. Savagian, "Separately Excited Synchronous Motor with Rotary Transformer for Hybrid Vehicle Application," *IEEE Energy Conversion Congress and Expo (ECCE)*, pp. 5844-5851, 2014.

[20] M. Aoyama and T. Noguchi, "Experimental Verification of Radial-Air-Gap-Type Permanent-Magnet-Free Synchronous Motor Utilizing Space Harmonics with Auxiliary Poles," *IEEJ Trans. on IA.*, vol. 135, no. 8, pp. 869-881, 2015. (in Japanese)

[21] M. Aoyama and T. Noguchi, "Permanent-Magnet-Free Synchronous Motor with Self-Excited Wound-Field Technique Utilizing Space Harmonics," *Applied Power Electronics Conference and Exposition (APEC)*, pp. 3187-3194, 2017.

[22] J. Dai and D. C. Ludois, "A Survey of Wireless Power Transfer and a Critical Comparison of Inductive and Capacitive Coupling for Small Gap Applications," *IEEE Trans. on Power Electronics*, vol. 30, no. 11, pp. 6017-6029, 2015.